This document is the accepted manuscript version of the paper:
PHYSICAL REVIEW A 89: Paper 053403. (2014)
DOI.: 10.1103/PhysRevA.89.053403

A simple model for describing resonance-enhanced strong field ionization with shaped ultrafast laser pulses

William D. M. Lunden, Péter Sándor, and Thomas C. Weinacht
Department of Physics and Astronomy, Stony Brook University, Stony Brook, New York 11794 USA

Tamás Rozgonyi
Institute of Materials and Environmental Chemistry,
Research Centre for Natural Sciences, Hungarian Academy of Sciences,
Magyar tudósok körútja 2, Budapest, HU-1117, Hungary

We present a simple model for calculating strong field atomic and molecular ionization dominated by Freeman resonances. Our model combines multiphoton coupling between bound states, including dynamic Stark shifts, with coupling to a discretized continuum. The simplicity of the model allows us to interpret pulse shape dependent strong field ionization yields and to demonstrate the relevance of strong field atomic/molecular phase matching to ionization as well as bound state population transfer. Comparison with experimental measurements demonstrates that the calculations capture the essence of the pulse shape dependent ionization yields.

I. INTRODUCTION

Strong field molecular ionization (SFI) is of great interest for many areas of ultrafast molecular science including following excited state molecular dynamics [1], probing molecular structure [2–5], high harmonic generation and attosecond science [6–9]. Because of its importance, there has been significant effort devoted to calculations of strong field moleclar ionization [10]. Multiphoton [11, 12] and quasi-static tunnel ionization [13–18] approaches have proven to be quite successful in describing many aspects of strong field ionization, such as intensity and angular dependent yields. Since strong field ionization can lead to the production of multiple ionic states [8, 19], and shaped laser pulses can control the ionization to different ionic states [20], there is a desire to understand the pulse shape dependent yield to different ionic states. While the calculations have captured many aspects of molecular SFI (angular dependence, ionization to different cationic states, intensity dependence etc), we argue that there is a need for simple models that can help interpret pulse shape dependent ionization measurements and yield insight into the dynamics of ionization process. Here we develop a simple model for resonance enhanced strong field ionization [21, 22] which describes the pulse shape dependent yield to different ionic states as measured using photoelectron spectroscopy. Our calculations allow for direct interpretation of pulse shape dependent yields that we measure in the case of the molecule CH_2BrI.

II. DERIVATION OF EQUATIONS

Our model is based upon the idea of adiabatic elimination to arrive at a Schrödinger equation for a small number of bound and continuum states. Elimination of all of the states which are not resonantly connected to the initial, intermediate and final states allows us to derive multiphoton couplings and Stark shifts between these states. While a detailed quantitative assessment of the criteria for adiabatic elimination for the molecules we consider experimentally would undoubtedly require the inclusion of more states than we include below, we limit ourselves to these representative states allowing us to capture the essence of the pulse shape dependent ionization dynamics. Including more resonant or off resonant states in the calculation is a straightforward extension of the derivation provided below.

In order to derive the Hamiltonian which we use to calculate resonance-enhanced strong field ionization, we start by considering an atomic or molecular system with field-free Hamiltonian H_0. We consider only electronic degrees of freedom for simplicity, although nuclear degrees of freedom can be included in a straightforward manner [23, 24]. We write the stationary bound states of this Hamiltonian as $|g\rangle$, $|n\rangle$, $|k\rangle$ and $|e\rangle$, where $|g\rangle$ and $|e\rangle$ are the ground state and the intermediate N photon resonant excited state, and $|n\rangle$ and $|k\rangle$ represent non-resonant intermediate states. We likewise write the wavefunction of a continuum state with energy E as $|u_E\rangle$. Figure 1 illustrates the energy levels and their coupling for a single continuum, although the equations are derived with multiple continua. While the derivation is for a single intermediate resonant state, the calculations can be easily extended to involve multiple intermediate states.

We expand the time-dependent wavefunction for the atom or molecule, $\Psi(t)$, as

$$\begin{aligned}\Psi(t) = c_g(t)|g\rangle e^{-i\omega_g t} + \sum_n c_n(t)|n\rangle e^{-i\omega_n t} \\ + \sum_k c_k(t)|k\rangle e^{-i\omega_k t} + c_e(t)|e\rangle e^{-i\omega_e t} \\ + \sum_u \int_0^\infty dE \Psi_u^{\text{ion}}(E,t)|u_E\rangle e^{-i\omega_u^{\text{ion}} t} \qquad (1)\end{aligned}$$

The total Hamiltonian is $H(t) = H_0 + V(t)$ with $V(t) = -\vec{\mu}\cdot\vec{E(t)}$, $\vec{\mu}$ being the transition dipole moment. In the

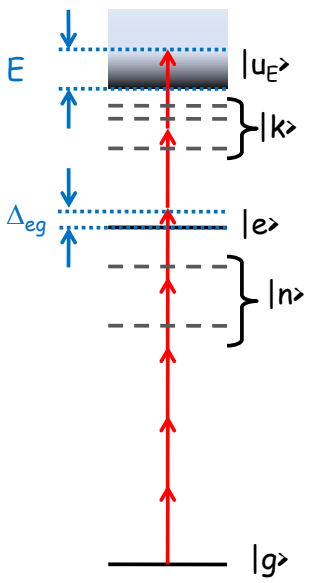

FIG. 1: Diagram illustrating energy levels considered in our calculations for a single continuum. While the diagram shows a single continuum for simplicity, the equations were derived for multiple continua. Symbols are defined in the text.

basis of the $|j\rangle$, $|u_E\rangle$ eigenstates it can be expressed as

$$\begin{aligned} H(t) = &\sum_j |j\rangle E_j \langle j| - \sum_{j,i} |j\rangle V_{ji}(t)\langle i| \\ &+ \sum_u \int_0^\infty dE |u_E\rangle (E_u^{ion} + U_p(t) + E)\langle u_E| \\ &- \left(\sum_{j,u} \int_0^\infty dE |u_E\rangle \tilde{V}_{ju}(E,t)\langle j| + \text{c.c.} \right) \end{aligned} \quad (2)$$

Here E_j is the eigenenergy of neutral state j, and E_u^{ion} is the eigenenergy of ionic state u. ($E_u^{ion} - E_0$ is the ionization potential for ionic state u). $U_p(t)$ is the ponderomotive energy, which is proportional to the intensity of the laser field and is the same for all ionic states. The V_{ji} and $\tilde{V}_{ju}$ are the matrix elements of the operator V(t). For the sake of simplicity, in the following we derive the model for the case of two photon transitions between $|g\rangle$ and $|e\rangle$, and $|e\rangle$ and the continuum. Accordingly, we assume that the matrix elements of V are nonzero only for couplings between $|g\rangle$ and $|n\rangle$, $|n\rangle$ and $|e\rangle$, $|e\rangle$ and $|k\rangle$, and $|k\rangle$ and $|u_E\rangle$. Generalizing the derivation to higher order couplings between the states which we explicitly consider in our calculations below is straightforward but tedious, which is why we only show the two photon coupling case here. For the case of higher order couplings one assumes as in the two photon case that there are no intermediate resonances between states.

Substituting equations 1 and 2 into the time-dependent Schrödinger equation, $i\hbar\dot{\Psi}(t) = H(t)\Psi(t)$, and exploiting the orthonormality of the basis states ($\langle i|j\rangle = \delta_{ij}, \langle u_E|u'_{E'}\rangle = \delta_{uu'}\delta(E-E')$), yields a set of coupled differential equations describing the time-dependent populations of the basis states:

$$\begin{aligned} i\hbar\dot{c_g} &= \sum_n V_{gn}c_n e^{-i\omega_{ng}t} \\ i\hbar\dot{c_n} &= V_{ng}c_g e^{i\omega_{ng}t} + V_{ne}c_e e^{-i\omega_{en}t} \\ i\hbar\dot{c_e} &= \sum_n V_{en}c_n e^{i\omega_{en}t} + \sum_k V_{ek}c_k e^{-i\omega_{ke}t} \\ i\hbar\dot{c_k} &= V_{ke}c_e e^{i\omega_{ke}t} + \sum_u \int_0^\infty \tilde{V}_{ku}(E)\Psi_u^{\text{ion}}(E)e^{-i\tilde{\omega}_{uk}t}dE \\ i\hbar\dot{\Psi}_u^{\text{ion}} &= (U_p + E)\Psi_{\text{ion}} + \sum_k \tilde{V}_{ku}(E)c_k e^{i\tilde{\omega}_{uk}t} \end{aligned} \quad (3)$$

Here $\omega_{ij} \equiv \omega_i - \omega_j = \frac{E_i - E_j}{\hbar}$ and $\tilde{\omega}_{uk} \equiv \omega_u^{\text{ion}} - \omega_k = \frac{E_u^{\text{ion}} - E_k}{\hbar}$. We assume that $\vec{\mu}_{ij} \cdot \hat{\epsilon} = \mu_{ij}$, where $\hat{\epsilon}$ is the polarization vector of a linearly polarized electric field.

We next consider an assumption on the matrix elements, $\tilde{V}_{ku}(E,t) = -\vec{\mu}_{ku}(E) \cdot \vec{E}(t)$, between neutral and continuum states: the transition dipole moment distributions $|\vec{\mu_{ku}}(E)| = \tilde{\mu}_{ku}$, i.e., they are independent of E if $0 < E < E_u^{\max}$, and they are zero otherwise. The parameter $E_u^{\max}$ is an upper limit placed on the photoelectron energy, which can be chosen arbitrarily as long as the spectral tail of the electric field is not truncated. As a next step, we expand the continuum state wavefunction in the basis of Legendre polynomials:

$$\Psi_u^{\text{ion}}(E,t) = \sum_{l=0}^{M\to\infty} \Phi_{l+1}^{(u)}(t)\sqrt{\frac{2l+1}{E_u^{\max}}} P_l\left(\frac{2E}{E_u^{\max}} - 1\right) \quad (4)$$

As has been discussed in previous work [24], using the recursion relations for Legendre polynomials it can be shown that the coefficients $\Phi_l^{(u)}(t)$ of the continuum state obey the TDSE and form a ladder of coupled states. $\Phi_1^{(u)}$ is coupled only to c_k and to $\Phi_2^{(u)}$, and in general $\Phi_l^{(u)}$ is coupled only to $\Phi_{l-1}^{(u)}$ and $\Phi_{l+1}^{(u)}$. Defining $\phi_l^{(u)} \equiv e^{i\frac{E_u^{\max}}{2\hbar}t}\Phi_l^{(u)}$, we may rewrite Equations 3 utilizing this ladder as:

$$\begin{aligned} i\hbar\dot{c_g} &= \sum_n V_{gn}c_n e^{-i\omega_{ng}t} \\ i\hbar\dot{c_n} &= V_{ng}c_g e^{i\omega_{ng}t} + V_{ne}c_e e^{-i\omega_{en}t} \\ i\hbar\dot{c_e} &= \sum_n V_{en}c_n e^{i\omega_{en}t} + \sum_k V_{ek}c_k e^{-i\omega_{ke}t} \\ i\hbar\dot{c_k} &= V_{ke}c_e e^{i\omega_{ke}t} + \sum_u V_{ku}\phi_1^{(u)} e^{-i\omega_{uk}t} \\ i\hbar\dot{\phi_1}^{(u)} &= \sum_k V_{ku}c_k e^{i\omega_{uk}t} + U_p\phi_1^{(u)} + \rho_2^{(u)}\phi_2^{(u)} \\ i\hbar\dot{\phi_l}^{(u)} &= U_p\phi_l^{(u)} + \left(\rho_l^{(u)}\phi_{l-1}^{(u)} + \rho_{l+1}^{(u)}\phi_{l+1}^{(u)}\right) \end{aligned} \quad (5)$$

where $\rho_l^{(u)} = \frac{(l-1)E_u^{\max}}{2\sqrt{4(l-1)^2-1}}$, $\omega_{uk} \equiv \tilde{\omega}_{uk} + \frac{E_u^{\max}}{2\hbar}$. Furthermore introducing the definition, $\mu_{ku} = \tilde{\mu}_{ku}\sqrt{E_u^{\max}}$, the $V_{ku} = \sqrt{E_u^{\max}}\tilde{V}_{ku}$.

We parameterize a pulsed electric field $\vec{E}(t)$ as

$$\vec{E}(t) = \frac{1}{2}\epsilon(t)e^{-i\omega_0 t}\hat{\epsilon} + \text{ c.c.}, \tag{6}$$

where

$$\epsilon(t) = \epsilon_0\sqrt{g(t)}e^{i\varphi(t)/2}, \tag{7}$$

ϵ_0 is the electric field amplitude, ω_0 is the central frequency of the laser pulse, $\varphi(t)/2$ is the temporal phase of the field, $g(t)$ is the temporal intensity envelope. We next substitute the dipole operator, using the parametrization given in Equation 6 into Equations 3 and adiabatically eliminate the states $|n\rangle$ and $|k\rangle$, as discussed in previous work [25], to derive multiphoton couplings between $|g\rangle$ and $|e\rangle$ and between $|e\rangle$ and $|u_E\rangle$. This adiabatic elimination is performed under the assumption that the transitions to the states $|n\rangle$ and $|k\rangle$ are far off-resonance. We furthermore invoke the multi-photon rotating wave approximation, and thus reduce Equations 3 to the following set of coupled differential equations:

$$\begin{aligned}
i\dot{c_g} &= \omega_g^{(s)}(t)c_g + \chi_{eg}^*(t)e^{i\Delta_{eg}t}c_e \\
i\dot{c_e} &= \chi_{eg}(t)e^{-i\Delta_{eg}t}c_g + \omega_e^{(s)}(t)c_e + \sum_u \chi_{ue}^*(t)e^{i\Delta_{ue}t}\phi_1^{(u)} \\
i\dot{\phi_1}^{(u)} &= \chi_{ue}(t)e^{-i\Delta_{ue}t}c_e + \left(\omega_u^{(s)}(t) + \frac{1}{\hbar}U_p(t)\right)\phi_1^{(u)} \\
&+ \frac{1}{\hbar}\rho_2^{(u)}\phi_2^{(u)} \\
i\dot{\phi_l}^{(u)} &= \frac{1}{\hbar}\left(U_p(t)\phi_l^{(u)} + \rho_l^{(u)}\phi_{l-1}^{(u)} + \rho_{l+1}^{(u)}\phi_{l+1}^{(u)}\right)
\end{aligned} \tag{8}$$

where $\omega_i^{(s)}$ is the dynamic Stark shift of the state i, χ_{ij} is the effective multi-photon Rabi frequency [32] for transitions between states i and j, $\Delta_{ij} \equiv N_{ij}\omega_0 - \omega_{ij}$ is the multi-photon detuning between states i and j, and * denotes complex conjugation. (Here i denotes g or e and j denotes either e or u.) While the derivation shown here is for the case of two photon coupling between $|g\rangle$ and $|e\rangle$, as well as $|e\rangle$ and $|u_E\rangle$, the final result is valid for higher order couplings with χ_{ij} given by $\chi_{0,ij}(\epsilon(t))^{N_{ij}}$, where $\chi_{0,ij}$ is a constant and N_{ij} is the photon order of the transition[33]. For the case of N_{ij}=2, and $\omega_i > \omega_j$, $\chi_{ij}(t)$ can be written explicitly as [25]:

$$\chi_{ij}(t) = -\sum_m \frac{\mu_{im}\mu_{mj}}{(2\hbar)^2}\frac{\epsilon_0^2 g(t)e^{i\varphi(t)}}{\omega_{mj} - \omega_0} \tag{9}$$

$\omega_i^{(s)}(t)$ is given by:

$$\omega_i^{(s)}(t) = -\sum_m \frac{\mu_{im}^2}{2\hbar^2}\epsilon_0^2 g(t)\frac{\omega_{mi}}{\omega_{mi}^2 - \omega_0^2}, \tag{10}$$

where m represents n or k (see figure 1).

The N photon rotating wave approximation means that we consider $N\hbar\omega \gg \Delta_{ij}$. For typical parameters in our calculations $\Delta_{ij} \sim 100$ THz, and $N\hbar\omega \sim 1900$ THz. For an appropriate choice of $E_u^{\max}$, $\Delta_{ue} \sim 0$, ensuring that the multi-photon rotating wave approximation is valid for the intermediate excited state to continuum transition as well. Calculations where we set $\omega_u^{(s)}(t)$ comparable $\omega_e^{(s)}(t)$ yielded very similar results to calculations where it was set to zero. We observed a small shift of the peak in the photoelectron spectrum (¡10 meV) as well as a small reduction (15 percent) in the yield. Since the effect on the calculations is small and we had no way to calculate this quantity *ab initio*, we set $\omega_u^{(s)}(t) = 0$ for the calculations shown below.

Equations 8 may then be rewritten in a more enlightening form by performing the following transformation:

$$\begin{aligned}
c_g &= b_g e^{-i\int_{-\infty}^t \omega_g^{(s)}dt'} \\
c_e &= b_e e^{-i\int_{-\infty}^t \omega_e^{(s)}dt'}
\end{aligned} \tag{11}$$

Applying this transformation to Equations 8, using the special condition for $E_u^{\max}$, which makes $\Delta_{ue} = 0$, and explicitly separating the temporal phase from the multiphoton couplings, $\Omega_{ij}(t)e^{iN_{ij}\varphi(t)/2} = \chi_{ij}(t)$, we get the following equations:

$$\begin{aligned}
i\dot{b_g} &= \Omega_{eg}(t)e^{i\alpha(t)}b_e \\
i\dot{b_e} &= \Omega_{eg}(t)e^{-i\alpha(t)}b_g + \sum_u \Omega_{ue}(t)e^{i\beta(t)}\phi_1^{(u)} \\
i\dot{\phi_1}^{(u)} &= \Omega_{ue}(t)e^{-i\beta(t)}b_e + \frac{1}{\hbar}\left(U_p(t)\phi_1^{(u)} + \rho_2^{(u)}\phi_2^{(u)}\right) \\
i\dot{\phi_l}^{(u)} &= \frac{1}{\hbar}\left(U_p(t)\phi_l^{(u)} + \rho_l^{(u)}\phi_{l-1}^{(u)} + \rho_{l+1}^{(u)}\phi_{l+1}^{(u)}\right)
\end{aligned} \tag{12}$$

where the molecule-field phase, $\alpha(t)$, and $\beta(t)$ are given by:

$$\begin{aligned}
\alpha(t) &= \Delta_{eg}t - \frac{N_{eg}}{2}\varphi(t) - \int_{-\infty}^t \delta_\omega^{(s)}(t')dt' \\
\beta(t) &= -\frac{N_{ue}}{2}\varphi(t) + \int_{-\infty}^t \omega_e^{(s)}(t')dt' \ .
\end{aligned} \tag{13}$$

Here $\delta_\omega^{(s)} \equiv \omega_e^{(s)} - \omega_g^{(s)}$ is the dynamic Stark shift between states $|g\rangle$ and $|e\rangle$.

When written in this form, Equations 12 reveal a simple, intuitive picture for maximizing the ionization yield - one would like to minimize the laser molecule phase advance while the multiphoton coupling between ground and intermediate states is large. This picture is similar to earlier work which considered multiphoton transitions between neutral states[26]. Since the coupling between $|e\rangle$ and $|u_E\rangle$ is stronger than the coupling between $|g\rangle$ and $|e\rangle$ (given the difference in multiphoton coupling orders and the density of states), ionization is limited by the rate at which population can be transferred from $|g\rangle$ to $|e\rangle$ [27]. In order to maximize this rate, the sign of the coupling should not change while the magnitude is large. Thus, the variation of α should be kept minimum while Ω_{eg} is large. We note that the transition between $|e\rangle$ and $|u_E\rangle$ is not so sensitive to the laser phase since there is not a well defined molecule field phase for this transition given the continuum of final states.

III. PARAMETER CONSTRAINTS AND CALCULATION DETAILS

The values of the parameters used in the calculations were dictated by experimental values and physically motivated constraints. The laser pulses in the computations had a Gaussian intensity profile with a FWHM of 40 fs and a peak intensity between 10^{12} and a few times 10^{13} W/cm^2, consistent with our experiments. The multiphoton Rabi frequencies were chosen to satisfy a number of constraints. One is that the calculations yield an ionization fraction of between 0.01 and 0.1 for an unshaped laser pulse, in agreement with experiments. Another is that the Rabi frequency coupling the ground and intermediate states should be smaller than the Rabi frequency coupling the intermediate state and continuum so that transfer to the continuum dominates over Rabi cycles between the two bound states. This is consistent with the higher photon order of the ground to intermediate coupling relative to the intermediate to continuum coupling and the general observation in resonance enhanced multiphoton ionization that for n+m photon ionization with n>m, the n^{th} order process is the rate limiting step. Similarly, the Rabi frequency between the intermediate state and continuum should be much smaller than the field-free coupling between continuum ladder states so that population transfer up the ladder dominates over Rabi cycling between the intermediate state and continuum. Finally, if the coupling between the intermediate state and the continuum was too high, then there was negligible resonance enhancement, and poderomotive shifting of the peak in the photoelectron spectrum. This set an upper limit on the intermediate to continuum Rabi frequency. Based on these considerations, the multiphoton Rabi frequency Ω_{eg} was chosen so that it reached a value of 1.22 THz at the peak of the pulse, and the multiphoton Rabi frequency Ω_{ue} was set to reach a value of 71 THz at the peak of the pulse. Calculations for a range of Rabi frequencies around these values were carried out. The ionization yield as a function of pulse shape and intensity was not sensitive to the exact values of the Rabi frequencies.

The results shown below were obtained with $E_u^{\rm ion} = 9.7$ eV (chosen to match the ionization potential of CH_2IBr) and an $E_u^{\rm max}$ of 2eV, which is well above the maximum photoelectron energy so that the spectrum is not clipped. Calculations for larger $E_u^{\rm max}$ yielded the same results.

The ponderomotive shift of the continuum states was set to 0.06 eV (14.4 THz) per TW/cm^2. The Stark shift of the excited state was set to be equal to the ponderomotive shift of the continuum, given the fact that Rydberg states tend to shift ponderomotively. We also performed additional calculations in which the Stark shift of the excited state was set to be greater or less than the ponderomotive shift. These calculations are described in detail in the appendix. The multiphoton detuning Δ_{eg} is the parameter which was most difficult to constrain with experimental measurements. Based upon measurements of the photoelectron spectrum as a function of intensity, we estimate that the Stark shift at which resonance occurs is about 100 $\pm$ 50 THz. Δ_{eg} was therefore set to 100 THz.

The continuum ladder was truncated at $M = 400$ to make the calculation computationally tractable. We chose to focus on 5+2 resonance enhanced ionization because measurements of the intensity dependent ionization yield for CH_2BrCl and CH_2BrI showed a fifth order dependence. However, calculations for 4+3, 6+1, 6+2, as well as 2+1 all showed qualitatively similar results. Therefore we argue that our discussion and interpretation is not particularly sensitive to the multiphoton order of the resonance.

IV. EXPERIMENTAL APPARATUS

The experiments make use of amplified pulses from a Titanium Sapphire laser system, producing 30 fs pulses with up to 1 mJ pulse energy at 1 kHz repetition rate. The central wavelength is 780 nm. The pulses are shaped by a custom-built AOM-based pulse shaper which has approximately 300 resolution elements over a 60 nm spectral bandwidth. The shaped pulses are focused into a vacuum chamber where they interact with the effusive molecular beam of the sample. Using an electrostatic lens, electrons produced from photoionization are velocity map imaged onto a dual stack MCP detector followed by a phosphor screen. The 2D image on the phosphor screen is captured and digitized by a CMOS camera interfaced with a personal computer. Measurements of the photoelectron velocity map images were made as a function of laser pulse shape and intensity.

V. RESULTS AND DISCUSSION

Figure 2 shows the calculated photoelectron spectrum for several different intensities in the case of direct 7 photon ionization and also 5+2 resonant enhanced ionization for the case of a single continuum chosen for simplicity. As is evident from the figure, the peak shifts as a function of intensity for direct ionization, but does not shift significantly in the case of resonance enhanced ionization, since ionization takes place predominantly at intensities for which the intermediate state is shifted into resonance, regardless of the peak intensity of the pulse. The shift of the peak in the case of direct ionization is about 80 meV, and about 20 meV for the case of resonant enhanced ionization.

This behavior is reflected in our experimental measurements as well. Figure 3 shows the measured photoelectron spectrum for several different intensities for the case of direct ionization of CS_2 and 5+2 Freeman resonance enhanced ionization of CH_2BrI. Note that, as with the calculations, the direct ionization peak shifts ponderomotively with laser intensity, while in the case of Freeman

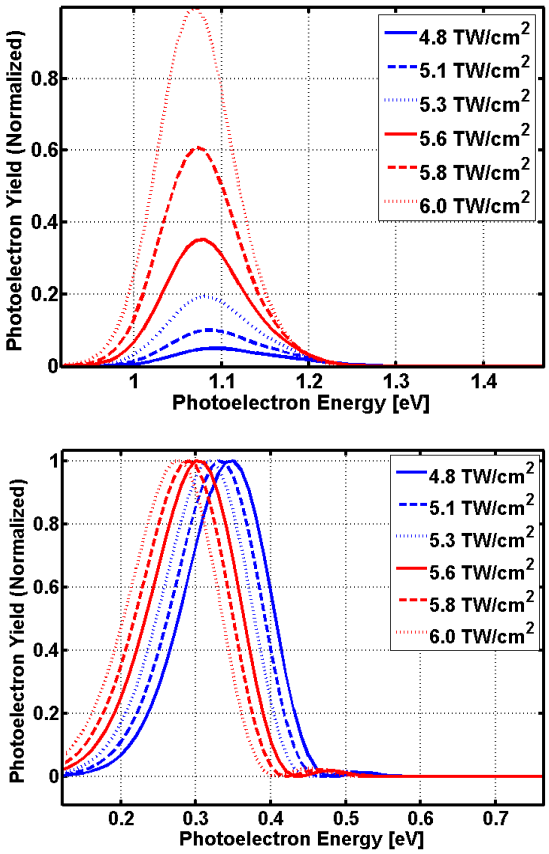

FIG. 2: Calculated photoelectron spectra using different laser intensities for 5+2 Freeman resonance mediated ionization (top panel) and direct 7 photon ionization (bottom panel). The results in the bottom panel are normalized to highlight the peak shift with intensity

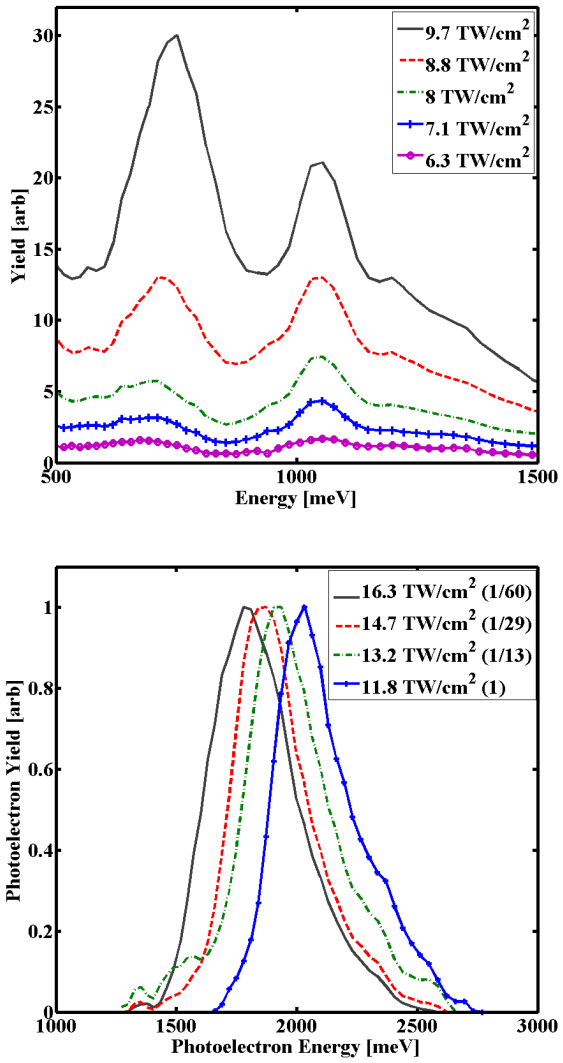

FIG. 3: Measured photoelectron spectra using different laser intensities for 5+2 Freeman resonance mediated ionization of CH_2BrI (top panel) and direct 9 photon ionization of CS_2 (bottom panel). As for the calculations, the results in the bottom panel are normalized to highlight the peak shift with intensity.

resonance enhanced ionization, the photoelectron peak does not shift with laser intensity [28]. The shift of the peaks in CH_2BrI is less than 40 meV, which is much less than the ponderomotive shift of 200 meV for the range of intensities represented by the data. The shift of the peak in figure 3 is about 250 meV, which is very close to the 270 meV ponderomotive shift for this range of intensities. Additional calculations carried out for different Stark shifts of the intermediate state (included in the appendix) show that for Stark shifts close to the ponderomotive shift, the peaks in the photoelectron spectrum do not shift very much with intensity. However, for negative Stark shifts the shift of the photoelectron peaks can be more substantial.

Having established that the calculations capture the behavior of the photoelectron spectrum for resonance enhanced and non-resonantly enhanced ionization, we next consider the pulse shape dependence of the ionization yield to a given continuum. We consider pulse shapes with a π spectral phase jump at a variable position in the spectrum. This paramaterization has proven to be effective in controlling multiphoton population transfer between bound states, with dynamics which can be interpreted in both the frequency and time domains [26, 29, 30]. Figure 4 shows the measured and calculated ionization yield as a function of π phase jump position for Freeman resonance enhanced ionization.

Both the measurements and the calculations show suppression of the ionization yield for π phase jumps near the center of the laser spectrum. This is largely because the peak intensity of the laser pulse drops below that which is required to bring the intermediate state into resonance, and the yield is greatly suppressed without the resonance enhancement. However, as shown in equation 13 and figure 5, the time dependent phase of the laser field also

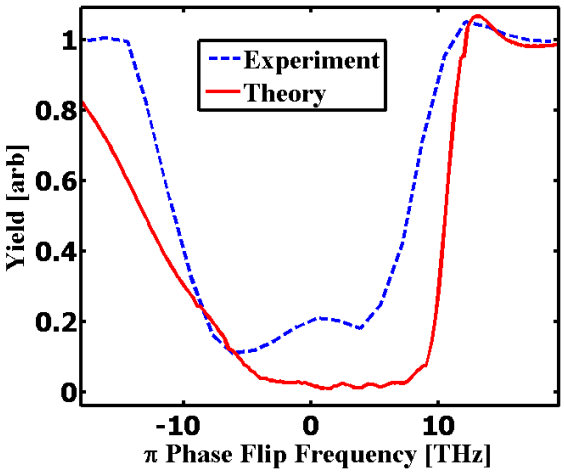

FIG. 4: Measured and calculated ionization yield as a function of π phase flip position.

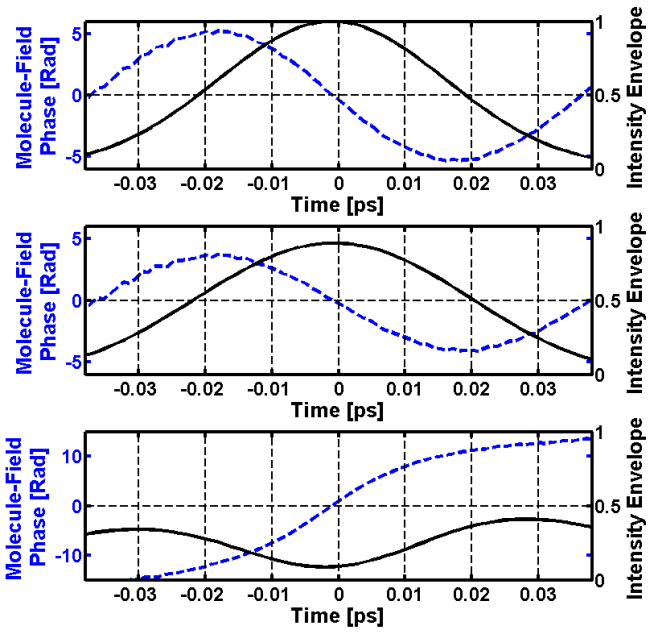

FIG. 5: Molecule-laser phase ($\alpha(t)$) and intensity profile ($I(t)$) for three different shaped pulses. The top panel shows $\alpha(t)$ and $I(t)$ for an unshaped laser pulse; the middle panel for an optimally shaped laser pulse which produces the maximum yield shown in figure 4; the bottom panel for a pulse with a π phase jump near the center of the spectrum, for which there is very little ionization yield.

plays a role in the ionization dynamics. This is discussed further in the appendix.

Motivated by earlier work [31], and equations 12, we look at the time dependence of $\alpha(t)$ and the intensity profile, $I(t)$, for pulses with π phase jump positions that maximize and minimize the ionization yield. Figure 5 shows the laser-molecule phase and intensity profile for three shaped pulses: an unshaped pulse, the one with the π phase jump position that yields the largest ionization yield (corresponding to the pulse shape that results in the slight increase above an unshaped pulse for both calculation and experiment in figure 4 when there is a π phase flip about 10 THz above the central freqeuncy), and the one with the π phase jump position which results in the lowest ionization yield. This figure illustrates the fact that the optimum pulse for ionization is the one which minimizes the laser-molecule phase evolution while the intensity (and consequently the multiphoton Rabi frequencies) are high, resulting in a large coupling between states [31]. By contrast, if the laser-molecule phase advances rapidly while the coupling between states is high, then there is very little ionization yield. These results highlight the importance of bound state dynamics in controlling the ionization yield because the phase advance between neutral states is well defined and one can control how this phase advances with respect to the laser field.

VI. CONCLUSIONS

The model we have developed represents the simplest combination of multiphoton coupling, dynamic Stark shifts and bound to continuum coupling which can describe pulse shape dependent strong field ionization. The simplicity of the model allows us to interpret the dynamics underlying the pulse shape dependence. The result is an intuitive picture of phase matching between dressed (i.e. Stark shifted) bound states and the laser pulse driving ionization.

VII. ACKNOWLEDGMENTS

The authors gratefully acknowledge support from the National Science Foundation under award number 1205397. Fruitful discussions with Philipp Marquetand and Matthias Ruckenbauer and support from COST Action CM1204 are also acknowledged.

VIII. APPENDIX

The calculations in figure 2 used a Stark shift equal to the ponderomotive shift. In order to test how sensitive the photoelectron spectrum is to the exact value of the Stark shift, we performed calculations of the photoelectron spectrum as a function of intensity for several different Stark shift values. These are shown in figure 6 for a range of Stark shifts from 0.85 times to 1.3 times the ponderomotive shift. The spectra are normalized to largest spectrum in panel d). One can see that there is very little shifting of the spectra with intensity for all

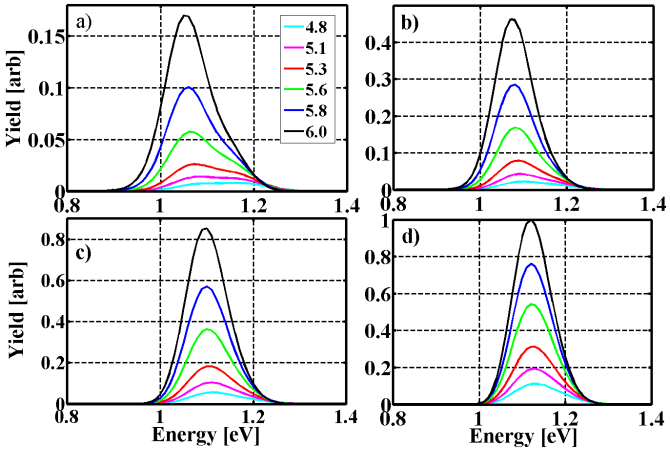

FIG. 6: Photoelectron spectra for different intensities with different Stark shifts of the intermediate state. Panel a) is for a Stark shift of 0.85 times the ponderomotive shift while panel b) is for 1.0 times the ponderomotive shift, panel c) is 1.15 times and panel d) 1.30 times the ponderomotive shift. The intensities for the different spectra are given in TW/cm^2 in the legend.

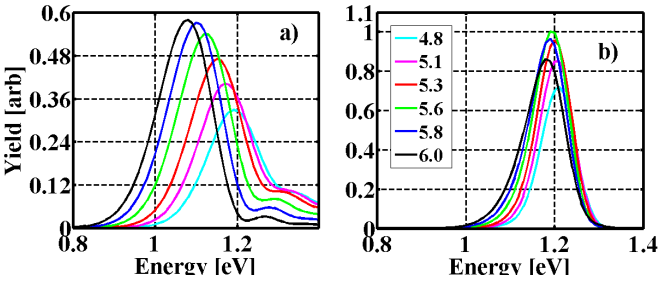

FIG. 7: Photoelectron spectra for negative (panel a) and positive (panel b) Stark shifts. The initial detuning of the intermediate state is 50 THz and the magnitude of the Stark shift is equal to the ponderomotive shift (0.06 eV per TW/cm^2). The legend indicates the intensities in TW/cm^2.

Stark shifts. The largest changes in the spectrum with intensity occur for the lowest intensity of the top left graph (panel a), which corresponds to the smallest Stark shift. In this case, the peak shifts and reshapes slightly because the pulse intensity is below resonance for the entire pulse duration, meaning that the ionization is not really resonance enhanced and therefore some shifting of the peak is to be expected.

To be quantitative about the results, we note that the ponderomotive shift of the peak for the range of intensities used in the calculations is about 100 meV. In comparison, for the case of a Stark shift of the intermediate state equal to the ponderomotive shift, the peak shift is 15 meV. For the case of an intermediate state Stark shift of 1.15 and 1.30 times the ponderomotive shift, the shift is 15 meV and 10 meV respectively. For the case of an intermediate state Stark shift 0.85 times the ponderomotive shift, the peak shifts by 0.25 meV. This is largely due to the fact that for such a low Stark shift the intermediate state never shifts into resonance during the pulse given the initial detuning. If the intermediate state doesn't shift into resonance, then one expects some ponderomotive shifting of the photoelectron peak since the ionization is not really resonance enhanced. Additional calculations show the peak shifting more significantly with intensity if the intermediate state remains far from resonance (i.e. several times the laser bandwidth) during the entire pulse.

Figure 7 shows a comparison of the photoelectron spectrum as a function of intensity for positive and negative Stark shifts (with the detuning also changing sign to ensure that the state always shifts into resonance rather than away from resonance). This figure illustrates that the photoelectron spectrum looks different for negative vs positive Stark shifts despite the fact that the total ionization yield in both cases is about the same. We argue that this is because the passage through resonance is not perfectly adiabatic and there is a slight delay between the population transfer from the ground state to the intermediate state and the ionization from the excited state. If the ionization is not strictly confined to times where the intermediate state is exactly resonant, then ionization at times when the intermediate state is off resonance will produce different photoelectron energies for the case of positive and negative detuning. This can be seen by comparing panels a) and b) of the figure. Panel a) shows the case of negative Stark shift (equal in magnitude to the ponderomotive shift) and an initial detuning of 50 THz. Given that the ponderomotive potential is 0.06 eV (14.4 THz) for 1 TW/cm^2, the intermediate state passes through resonance for all of the peak intensities considered in the plot. Panel b) shows the same calculation but for the case of equal and opposite Stark shift and detuning. While the peak shift with intensity in panel b) is less than 30 meV, it is greater than 100 meV for panel a). The peak in panel a) shifts to lower energy because any ionization which takes place after the intermediate state passes through resonance comes from an intermediate state which is Stark shifting to lower energies - in the opposite direction of the continuum. On the other hand, for the case of a positive Stark shift, the intermediate state is shifting along with the continuum, and so any ionization not taking place exactly at resonance leads to the same photoelectron energy as ionization at resonance.

In order to highlight the importance of the time dependent phase of the laser field as suggested by the expression in formula 13, we performed a calculation which compared the ionization yield for two pulses - one which had the time dependent intensity and phase associated with a spectral π phase flip and one which had only the time dependent intensity (i.e. no temporal phase variation). These calculations are shown in figure 8 and show that the enhancements in the yield near 12 THz and -11 THz are different for the two cases, illustrating the fact that the temporal phase of the laser can play an impor-

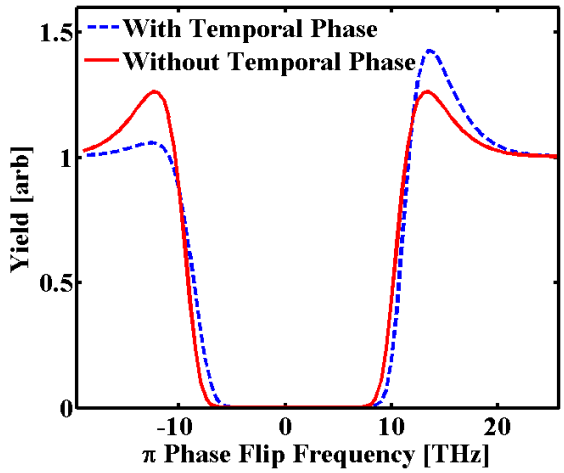

FIG. 8: Ionization yield as a function of π phase flip position for two pulses. One is a pulse with the time dependent intensity and phase associated with a π spectral phase flip whereas the other is a pulse with the same time dependent intensity but no temporal phase variation - i.e. the temporal phase associated with the π phase flip in the spectrum was removed.

tant role in the dynamics and lead to greater ionization yield than for an unshaped laser pulse.

[1] W. Li, A. Jaroń-Becker, C. Hogle, V. Sharma, X. Zhou, A. Becker, H. Kapteyn, and M. Murnane, Proceedings of the National Academy of Sciences **107**, 20219 (2010).
[2] M. Kotur, T. C. Weinacht, C. Zhou, and S. Matsika, Phys. Rev. X **1**, 021010 (2011).
[3] O. Smirnova, Y. Mairesse, S. Patchkovskii, N. Dudovich, D. Villeneuve, P. Corkum, and M. Y. Ivanov, Nature **460**, 972 (2009).
[4] J. Itatani, J. Levesque, D. Zeidler, H. Niikura, H. Pepin, J. Kieffer, P. Corkum, and D. Villeneuve, Nature **432**, 867 (2004).
[5] S. Patchkovskii, Z. Zhao, T. Brabec, and D. Villeneuve, Phys. Rev. Lett. **97**, 123003 (2006).
[6] P. Agostini and L. DiMauro, Reports on Progress in Physics **67**, 813 (2004).
[7] E. Goulielmakis, Z. Loh, A. Wirth, R. Santra, N. Rohringer, V. Yakovlev, S. Zherebtsov, T. Pfeifer, A. Azzeer, S. R. L. Kling, M.F. Kling, et al., Nature **466**, 739 (2010).
[8] A. E. Boguslavskiy, J. Mikosch, A. Gijsbertsen, M. Spanner, S. Patchkovskii, N. Gador, M. J. J. Vrakking, and A. Stolow, Science **335**, 1336 (2012).
[9] M. Kling and M. Vrakking, Annu. Rev. Phys. Chem. **59**, 463 (2008).
[10] M. Ivanov, M. Spanner, and O. Smirnova, Journal of Modern Optics **52**, 165 (2005).
[11] F. Faisal, Journal of Physics B **6**, L89 (1973).
[12] R. M. Potvliege, E. Mese, and S. Vucic, Physical Review A **81** (2010).
[13] B. Pickup, Chemical Physics **19**, 193 (1977).
[14] X. M. Tong, Z. X. Zhao, and C. D. Lin, Phys. Rev. A **66**, 033402 (2002).
[15] M. V. Ammosov, N. B. Delone, and V. P. Krainov, Sov. Phys. JETP **64**, 1191 (1986).
[16] A. Perelomov, V. Popov, and M. Terent'ev, Soviet Journal of Experimental and Theoretical Physics **23**, 924 (1966).
[17] L. V. Keldysh, Sov. Phys. JETP **20**, 1307 (1965).
[18] H. R. Reiss, Phys. Rev. A **22**, 1786 (1980).
[19] G. N. Gibson, R. R. Freeman, and T. J. McIlrath, Physical Review Letters **67**, 1230 (1991).
[20] D. Geißler, T. Rozgonyi, J. González-Vázquez, L. González, S. Nichols, and T. Weinacht, Physical Review A **82** (2010).
[21] T. Marchenko, H. G. Muller, K. J. Schafer, and M. J. J. Vrakking, Journal Of Physics B **43** (2010).
[22] G. N. Gibson, R. R. Freeman, T. J. McIlrath, and H. G. Muller, Phys. Rev. A **49**, 3870 (1994).
[23] M. Seel and W. Domcke, The Journal of Chemical Physics **95**, 7806 (1991).
[24] T. Rozgonyi, A. Glass, and T. Feurer, Journal of Applied Physics **88**, 2936 (2000).
[25] C. Trallero-Herrero, D. Cardoza, T. C. Weinacht, and J. L. Cohen, Phys. Rev. A **71**, 013423 (2005).
[26] C. Trallero-Herrero and T. C. Weinacht, Phys. Rev. A **75**, 063401 (2007).
[27] A. Markevitch, D. Romanov, S. Smith, H. Schlegel, M. Ivanov, and R. Levis, Physical Review A **69** (2004).
[28] P. Bucksbaum, R. Freeman, M. Bashkansky, and T. McIlrath, Journal of the Optical Society of America B **4**, 760 (1987).
[29] N. Dudovich, B. Dayan, S. M. Gallagher-Faeder, and Y. Silberberg, Phys. Rev. Lett. **86**, 000047 (2001).
[30] D. Meshulach and Y. Silberberg, Phys. Rev. A **60**, 1287 (1999).
[31] C. Trallero-Herrero, J. L. Cohen, and T. Weinacht, Phys.

Rev. Lett. **96**, 063603 (2006).
[32] The $\chi_{ij} \approx \chi_{ji}^*$ for small detuning, Δ_{ij}, and are exactly the same for $\Delta_{ij} = 0$.
[33] We note that $\chi_{0,ue}$ is proportional to $\sqrt{E_u^{\max}}$ for any photon order N_{ue} and $\omega_u^{(s)}(t)$ also dependent on $E_u^{\max}$.